J Mater Sci (2011) 46:6596–6602
DOI 10.1007/s10853-011-5608-3

Microscale characterization of granular deformation near a crack tip

Helena Jin · Wei-Yang Lu · Sandip Haldar · Hugh A. Bruck

Received: 11 April 2011 / Accepted: 3 May 2011 / Published online: 15 May 2011

Abstract This paper presents a study of microscale plastic deformation at the crack tip and the effect of microstructure feature on the local deformation of aluminum specimen during fracture test. Three-point bending test of aluminum specimen was conducted inside a scanning electron microscopy (SEM) imaging system. The crack tip deformation was measured in situ utilizing SEM imaging capabilities and the digital image correlation (DIC) full-field deformation measurement technique. The microstructure feature at the crack tip was examined to understand its effect on the local deformation fields. Microscale pattern that was suitable for the DIC technique was generated on the specimen surface using sputter coating through a copper mesh before the fracture test. A series of SEM images of the specimen surface were acquired using in situ backscattered electronic imaging (BEI) mode during the test. The DIC technique was then applied to these SEM images to calculate the full-field deformation around the crack tip. The grain orientation map at the same location was obtained from electron backscattered diffraction (EBSD), which was superimposed on a DIC strain map to study the relationship between the microstructure feature and the evolution of plastic deformation at the crack tip. This approach enables to track the initiation and evolution of plastic deformation in grains adjacent to the crack tip. Furthermore, bifurcation of the crack due to intragranular and intergranular crack growth was observed. There was also localization of strain along a grain boundary ahead of and parallel to the crack after the maximum load was reached, which was a characteristic of Dugdale–Barenblatt strip-yield zone. Thus, it appears that there is a mixture of effects in the fracture process zone at the crack tip where the weaker aspects of the grain boundary controls the growth of the crack and the more ductile aspects of the grains themselves dissipate the energy and the corresponding strain level available for these processes through plastic work.

H. Jin (✉) · W.-Y. Lu
Mechanics of Materials, Sandia National Laboratories, Livermore, CA, USA
e-mail: hjin@sandia.gov

S. Haldar · H. A. Bruck
Department of Mechanical Engineering, University of Maryland, College Park, MD, USA

Introduction

In earlier work [1], mechanism-based cohesive zone relations were developed to model the fracture process in ductile materials. These cohesive zone relations were combined with integration schemes to simulate the evolution of the plastic zones surrounding the moving crack tip. Attempts have also been made to experimentally map the displacement field at the crack tip during fracture tests based on the analysis of the electron backscattered diffraction (EBSD) patterns [2] from scanning electron microscopy (SEM) images. However, the digital camera inside the SEM system was unable to capture the necessary pattern details to distinguish the deformation fields for the specimens associated with different levels of plastic deformation. Therefore, there is a need for reliable technique to characterize crack tip local deformation at the microscale during fracture test to understand the relationship between the microstructure features and the evolution of plastic deformation associated with the mechanisms that give rise to the fracture process zone.

Digital image correlation (DIC) is a full-field deformation measurement technique that uses random speckle

patterns on the surface of a specimen to track the deformation via correlating the digitized undeformed and deformed images. It was originally proposed and used by researchers at the University of South Carolina [3–7]. The DIC technique has become a popular method in the *Experimental Mechanics* community for measuring surface displacements in a wide range of applications. Suitable patterns are very critical for DIC to obtain correct deformation results. At the micro-scale, the DIC pattern creation method is unique depending on the individual application and material. For example, they can be original microstructural surface features of the specimen (i.e., texture) or externally applied onto the specimen surface by various methods. Researchers have studied various techniques, such as air brushing, deposition of fluorescent nanoparticle, imprinted gold web, chemical deposition, and sputtering [8–11], to develop DIC patterns at the reduced scales.

Recently, SEM imaging has been combined with DIC technique to study spatial and drift distortion of SEM imaging [12, 13]. The SEM imaging incorporated with DIC technique has been successfully applied to study the mechanical behavior of LIGA specimens [14]. Some preliminary research was also conducted to investigate the crack tip deformation during fracture testing by combining the grid method and the DIC technique with SEM imaging. It was observed that the deformation at the crack tip might not be consistent with the linear elastic fracture mechanics (LEFM) solution, possibly due to the large plastic deformation as well as microstructure features [15]. This work is aimed at developing a systematic experimental method to measure the microscale crack tip deformation and to study the effect of microstructure features on the evolution of plastic deformation. A three-point bending stage was designed to fit into the SEM imaging system to conduct in situ fracture test. The SEM imaging capability was combined DIC technique to characterize the microscale crack tip deformation. In this paper, the fracture testing system and specimen, pattern generation technique and the image acquisition are presented in the experimental methods session. The DIC analysis of the images and the microstructure analysis are discussed in the experimental results session, and the resulting evolution of plastic deformation and associated mechanisms are then described.

Experimental methods

Fracture test configuration and specimen

Figure 1 shows the fracture testing system which consists of the SEM imaging system and the three-point bending stage inserted into the SEM. The SEM system is a JSM-840A from JOEL Corporation. The loading stage was installed inside the JSM-840A imaging system, replacing the original SEM chamber door. The load was measured with a force transducer mounted next to the specimen fixture on the stage, and the crosshead displacement was measured with a linear displacement sensor (LDS) at the end of the loading stage outside the chamber. The loading stage was capable of applying a tensile or compressive load of up to 1090 N to a specimen either by motor driven or manual driven gears. Three-point bending fracture test was thus conducted inside the SEM chamber where the SEM images could be acquired at each incremental step of loading.

The material of interest for this study was Al 6061-T651. Based on both the load capacity and space limitations of the SEM loading stage, fracture specimen was designed with a width of 12.5 mm (0.50″), length of

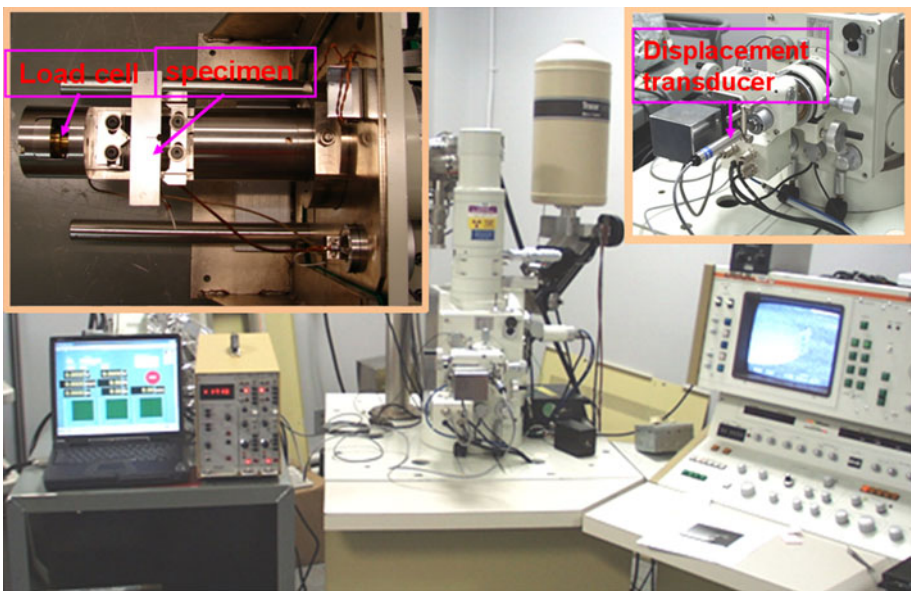

Fig. 1 Fracture test configuration using SEM and three-point bending stage

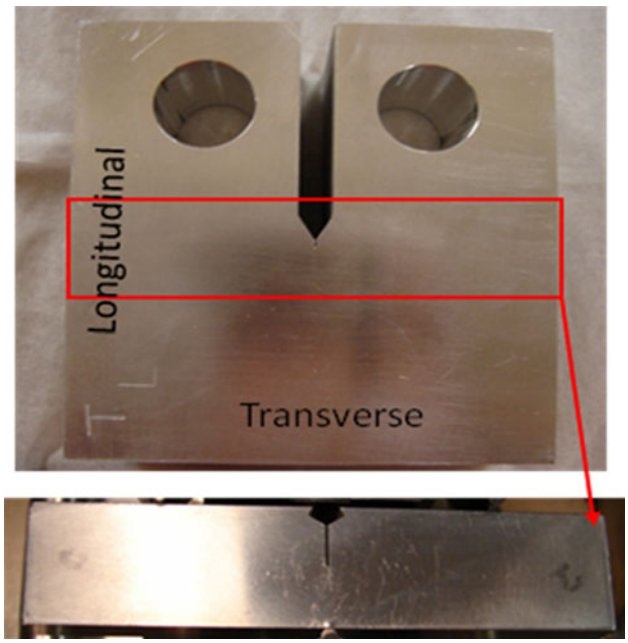

Fig. 2 CT specimen and three-point bending test specimen cut from CT specimen

76.2 mm (3.0″), span of 50.0 mm (2.0″), thickness of 6.25 mm (0.25″), and pre-crack length of 6.25 mm (0.25″). The pre-crack was generated from a larger compact tension (CT) specimen along the longitudinal direction of the specimen. The three-point bending specimen was then extracted from the CT specimen using the electro-discharge machining (EDM). The CT specimen and three-point bending fracture specimen are shown in Fig. 2. The specimen surface was mechanically polished up to a 3 μm finish and ultrasonically cleaned. The specimen was then electro polished to remove surface marks to impart a smooth and flat surface.

Generation of microscale patterns for DIC technique at the crack tip

In this experiment, a previously developed technique was adopted to generate pattern at the crack tip on the fracture specimen [14]. After final polish, the pre-crack of the fracture specimen could be observed under optical microscope. A copper grid with 2000 mesh (G2000HS from Ted Pella, Inc. [16]) was carefully laid over the specimen surface to cover the tip of the pre-crack. Special care was needed to handle the mesh grid to ensure uniform flat contact between the mesh grid and the specimen surface such that the grid pattern could be nicely transferred onto the specimen surface. Figure 3a shows an optical image of copper grid covering the crack tip. After careful layout of the copper mesh grid, the specimen was then placed into a sputtering system, where a thin layer of gold film with approximate 20 nm of thickness was sputter coated. Thus, the area underneath the mesh bar was covered and the space between the mesh bars was coated with gold film. The mesh grid pattern was therefore transferred onto the specimen surface. The pitch size of the mesh was 12.5 μm and the width of the mesh bar was 5 μm. Figure 3b shows an SEM image of the transferred grid pattern on the specimen.

Acquisition of SEM images during the fracture test

To apply the DIC technique for calculating the displacement fields, a gray scale variation is required within each subset and the pattern must be stable during imaging. Based on our previous research [14], it was found out that backscattered electronic imaging (BEI) mode could generate nice image contrast based on the difference in the atomic number between the aluminum specimen and the coated gold film on the specimen surface. BEI was less sensitive to the surface topography than secondary electronic imaging (SEI) mode. Thus, the BEI mode was adopted to acquire images during the three-point bending test. A typical image of the crack tip at the original undeformed step is shown in Fig. 4a. One can see that the grid pattern has been nicely transferred onto the specimen surface by sputter coating. To have random gray scale patterns for DIC, the intensity of the pixels inside each individual grid of the mesh was adjusted to have variation

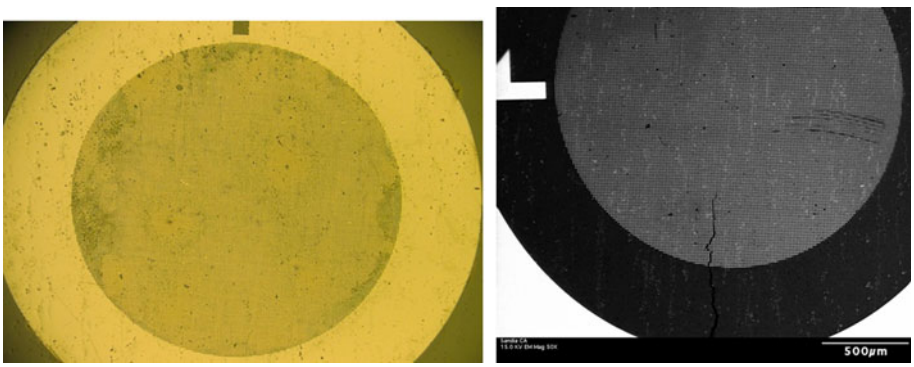

Fig. 3 Optical image of the copper grid laid over the pre-crack and SEM image of the transferred grid pattern showing the crack tip position relative to the grid

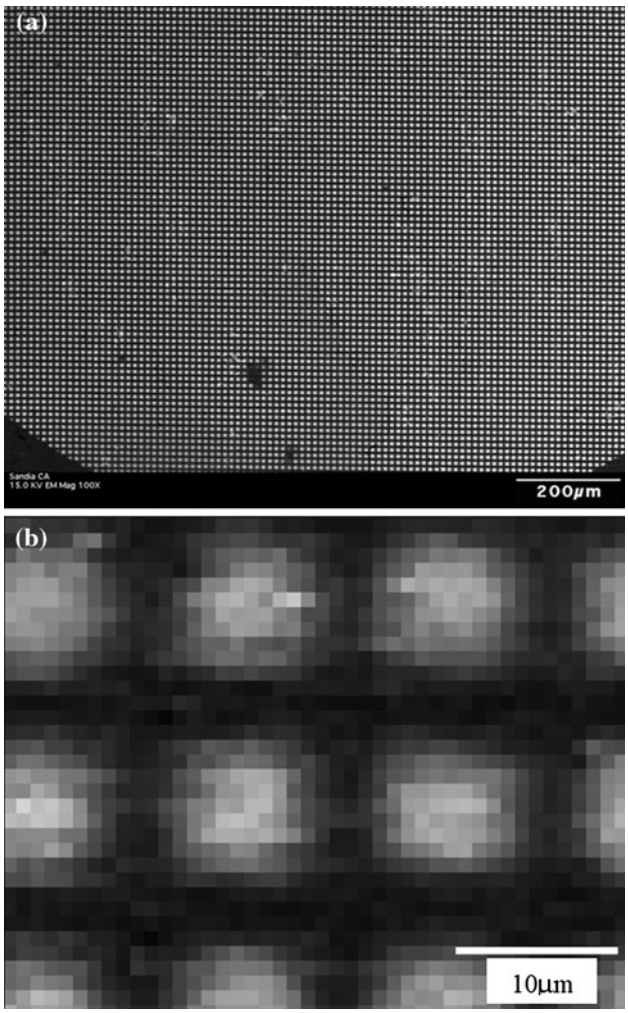

Fig. 4 **a** A typical image at the original undeformed step acquired using BEI mode; **b** *gray scale* variation within each individual grid

as shown in Fig. 4b. The imaging parameters were thus adjusted to achieve the optimal brightness and contrast for DIC.

The load versus displacement curve for a three-point bend fracture test obtained from the load cell and displacement transducer for the testing fixture is shown in Fig. 5. SEM images of the specimen were acquired in situ after each step of loading using the BEI mode. A magnification of 100× was used for SEM imaging since it was determined at this magnification the area of interest would encompass the region around the crack tip where plastic deformation would occur. The pixel resolution used in the SEM imaging was, therefore, the spatial resolution of each pixel was 0.85 μm and the imaging area was 1150 × 980 μm^2. The pitch size of the mesh was 12.5 μm and the bar width of the mesh was 5 μm. This resulted in each individual mesh grid being about 15 × 15 $pixels^2$. Figure 6a–d shows the grayscale BEI of the sputter coated patterns around the crack tip at different deformed states

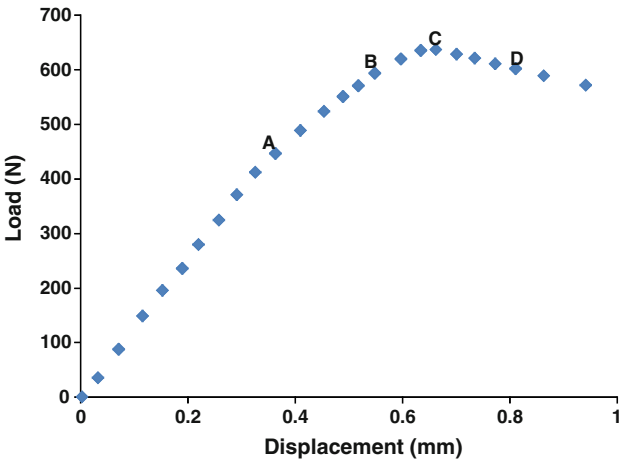

Fig. 5 Load versus displacement of the three-point bending test

marked as A, B, C, and D in the load versus displacement curve in Fig. 5. One can clearly see that the crack begins to open up significantly at the later stages as the specimen begins to experience significant plastic deformation, as evidenced by the load–displacement curve becoming nonlinear. After each step of loading, the imaging area on the specimen was carefully relocated to its origin using higher magnification to minimize the spatial distortion from SEM imaging.

Experimental results

Grain orientation map of the specimen

To study the effect of microstructure features on the crack tip deformation, the grain orientation map of the specimen around the crack tip was obtained using EBSD before the fracture test. The EBSD data were acquired at a magnification of 200× to particularly focus on the grains closest to the crack tip. Figure 7a shows the grain orientation color map of the area around the crack tip. Figure 7b is the corresponding pattern quality map that was overlaid with BEI of the mesh grid. The EBSD pattern quality could be influenced by a number of factors including local crystalline perfection, phase and orientation, etc. and was often able to reveal features such as grain and grain boundary. The pattern quality map in Fig. 7b clearly shows the grain and grain boundary information at the crack tip.

Full-field analysis of the deformation at the crack tip

The BEI of the specimen were recorded in situ after each incremental step of the loading. The DIC software ARAMIS was successfully applied to these images to calculate the displacement field. The mesh grid size was about

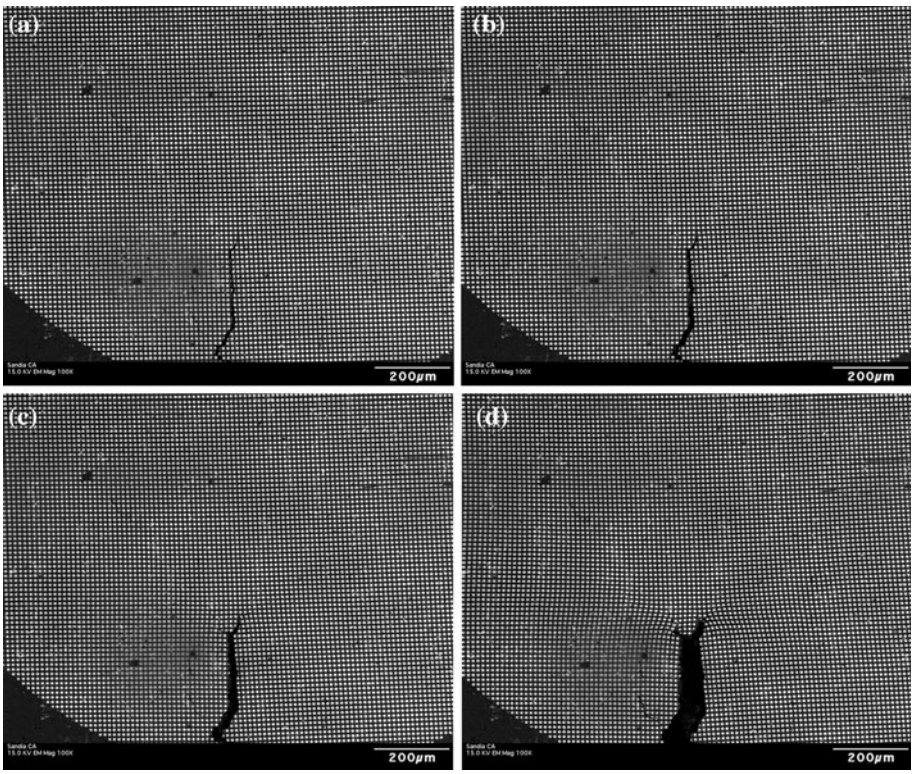

Fig. 6 A series of BEI at the selected loading steps as marked in Fig. 5, **a** step 10, **b** step 15, **c** step 18, and **d** step 23

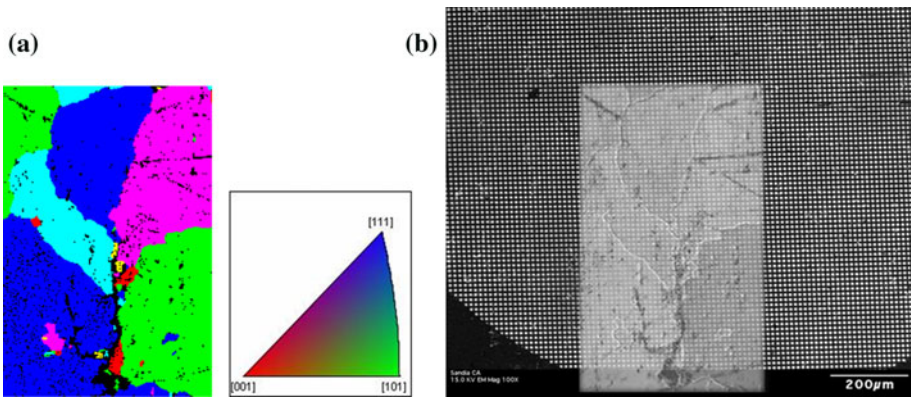

Fig. 7 **a** Grain orientation map around crack tip at 200×, **b** corresponding pattern quality map overlaid onto crack tip

15 × 15 pixels^2 and image size was 1350 × 1150 pixels^2. Therefore, the subset size of 25 × 25 pixels^2 and step size of 5 pixels were chosen for DIC analysis. The Von Mises effective strain distributions for the steps in Fig. 6a–d were overlaid with the grain orientation map as shown in Fig. 8a–d. It is clearly observed how the strain concentrations at the crack tip were developed during the incremental loading. At an early stage of loading, as shown in Fig. 8a, there is small-scale yielding to the right side along a branch of the crack tip at an approximate angle of 50° with respect to the crack direction, but the strain field appears to be predominantly elastic, which was consistent with the load–displacement curve. In Fig. 8b, the strain field indicates the evolution of more significant plastic deformation. The strain field shape is overall consistent with the classical HRR field [17–19] except for the slight asymmetry most likely due to grain orientation effects. The crack growth and propagation along the original pre-crack direction in front of the crack tip was ceased and crack tip branching was observed. Figure 8c shows the strain distribution at the maximum load. It can be clearly seen that the strain distribution has spread further from the crack tip than earlier stages. However, as the strain concentration spreads beyond the grains adjacent to the crack on the left hand side, the plastic strains begin to develop within the next grain rather than continuously across the grain boundary. Figure 8d shows the strain distribution for loading step D after the maximum load. The strain

concentrations between adjacent grains on the left hand side have coalesced, however, a new strain concentration area along the grain boundary parallel to the crack can also be observed as marked with a circle.

The above observations of the initiation and evolution of strain fields and crack growth at the microscale can be understood from the overlay of the grain map and strain field at the crack tip in Fig. 8 as follows.

(1) *Crack tip branching*: This is most likely caused by the orientation of the grain in front of the crack tip which prevents intragranular propagation of the crack, and instead favors intergranular crack growth along weaker grain boundaries or intragranular growth within a grain adjacent to the crack whose orientation was in a more favorable direction for crack growth. However, it does not appear that the bifurcation had a significant influence on the evolution of the strain distribution with only slight perturbations very close to the crack tip.

(2) *Evolution of strain field*: The deformation concentration is first developed at the crack tip at the early stage of loading. Initially, the shape of the strain field within grains adjacent to the crack is consistent with the prediction of classical HRR theory at the continuum scale, though the exact shape may vary depending on the yielding behavior of the specific material, which is not within our research interests. A slight asymmetry of the strain field is observed, which may be caused by the grain boundary orientation. As the strain field evolved, there is a discontinuous concentration of strain across the grain boundary. This is most likely due to orientation effects of the grain adjacent where there is resistance to plastic deformation at the grain boundary due to dislocation motion, but with sufficient critical resolved shear stress to allow for dislocation motion within the grain.

(3) *Strain concentration ahead of the crack*: After the maximum load is reached, strain is concentrated in a strip along a weaker grain boundary in front of and parallel to the crack, similar to a Dugdale–Barenblatt strip-yield zone [20, 21].

The experimental results in Fig. 8 showed that the shape of the microscale plastic strain fields at the crack largely conformed to the predictions of HRR theory at the continuum scale. However, microstructure features, such as grain orientation, grain size, etc., cause the evolution to be non-uniform. Furthermore, the eventual growth of the crack appears to be controlled by the level of deformation necessary to propagate the crack along the weaker grain boundaries ahead of it while the evolution of the strain fields tends to limit the level of strain and to dissipate the energy available for crack growth through plastic work. Thus, it is anticipated that these findings will have important consequences on the development of fundamental microscale models for predicting R curve behavior in metals.

The above experiments demonstrated that the technique combining SEM imaging and DIC was able to successfully measure the microscale granular deformations at the crack

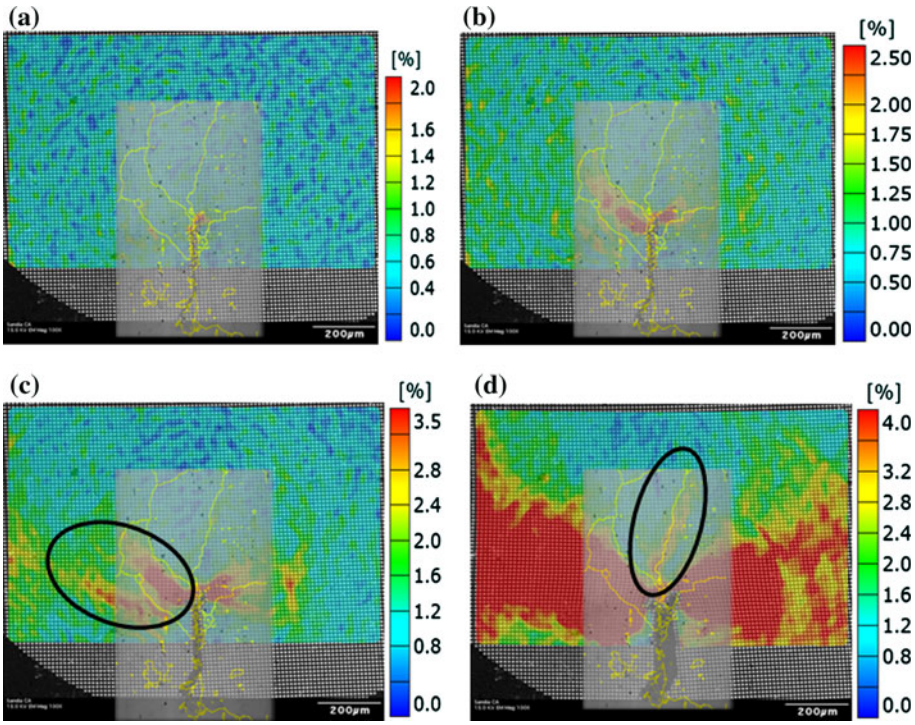

Fig. 8 The grain boundary map overlaid on the Von Mises strain fields obtained at steps (A)–(D) in Fig. 5

tip. Using various magnifications of SEM imaging, this technique can be extended for applications with a wide range of scales. With higher magnification of SEM imaging, this technique can be applied to quantitatively characterize the deformation and cracking behavior of nanocomponents in nanofabrication as what has been observed by Li et al. [22]. These quantitative measurements in return will guide the nanofabrication process and improve the performance of the fabricated nanodevices.

Conclusions

A new method combining SEM imaging with the DIC full-field displacement measurement technique was successfully applied to study microscale plastic deformation at the crack tip during fracture test of Al specimen. The BEI mode was able to acquire consistent images which were suitable for the DIC technique during three-point bending fracture test. DIC analysis of the BEI provided detailed strain distribution information at the crack tip. The local grain maps obtained from EBSD were carefully overlaid onto the strain fields, which provided valuable insight into microstructure effect on the evolution of strain localization at the crack tip due to plastic deformation. It was found out that plastic strain initially accumulated within grains adjacent to the crack tip with a shape consistent with HRR field predictions, which then evolve discontinuously across grain boundaries. Bifurcation of the crack tip along weaker grain boundaries and within more favorably oriented grains caused only slight perturbations in these fields very close to the crack tip. There was also development of a more classical Dugdale–Barenblatt strip-yield zone in a grain boundary ahead of and parallel to the crack after the maximum load was reached. Thus, it appears that there is a mixture of effects in the plastic deformation at the crack tip where the weaker aspects of the grain boundary controls the growth of the crack and the more ductile aspects of the grains themselves dissipate the energy and the corresponding strain level available for this growth process through plastic work. These findings have important consequences on the development of fundamental microscale models for predicting R curve behavior in metals. The technique combining SEM imaging with DIC has a great promise in a wide range of applications.

Acknowledgements Sandia National Laboratories is a multi-program laboratory managed and operated by Sandia Corporation, a wholly owned subsidiary of Lockheed Martin Corporation, for the U.S. Department of Energy's National Nuclear Security Administration under contract DE-AC04-94AL85000. Support provided by NSF under grant number DMR-0907122 is also greatly appreciated.

References

1. Klein PA, MacFadden SX, Bammann DJ, Hammi Y, Foulk JW, Antoun BR (2003) Sandia Report, SAND 2003-8804
2. Wilkinson AJ, Hirsch PB (1997) Micron 28:279
3. Peters WH, Ranson WF (1982) Opt Eng 21:432
4. Sutton MA, Wolters WJ, Peters WH, Ranson WF, McNeill SR (1983) Image Vis Comput 1(3):133
5. Chu TC, Ranson WF, Sutton MA, Peters WH (1985) Exp Mech 25(3):232
6. Sutton MA, Cheng M, Peters WH, Chao YJ, McNeill SR (1986) Image Vis Comput 4(3):143
7. Bruck HA, McNeill SR, Sutton MA, Peters WH (1989) Exp Mech 29:261
8. Berfield TA, Patel JK, Shimmin RG, Braun PV, Lambros J, Sottos NR (2007) Exp Mech 47(1):51
9. Scrivens WA, Luo Y, Sutton MA, Collette SA, Myrick ML, Miney P, Colavita PE, Reynolds AP, Li X (2007) Exp Mech 47(1):63
10. Collette SA, Sutton MA, Miney P, Reynolds AP, Li XD, Colavita PE, Scrivens WA, Luo Y, Sudarshan T, Muzykov P (2004) Nanotechnology 15(12):1812
11. Sun ZL, Lyons JS, McNeill SR (1997) Opt Lasers Eng 27(4):409
12. Sutton MA, Li N, Joy DC, Reynolds AP, Li X (2007) Exp Mech 47(6):775
13. Sutton MA, Li N, Garcia D, Cornille N, Orteau JJ, McNeill SR, Schreier HW, Li X, Reynolds AP (2007) Exp Mech 47(6):789
14. Jin H, Lu WY, Korellis J (2008) J Strain Anal Eng Des 43(8):719
15. Jin H, Haldar S, Bruck HA, Lu WY (2011) Exp Mech. doi: 10.1007/s11340-010-9459-7
16. http://www.tedpella.com/grids_html/gilder2.htm#g2000hs
17. Hutchinson JW (1968) J Mech Phys Solids 16:13
18. Hutchinson JW (1968) J Mech Phys Solids 16:337
19. Rice JR, Rosencren GF (1968) J Mech Phys Solids 16:1
20. Dugdale DS (1960) J Mech Phys Solids 8:100
21. Barenblatt GI (1962) Adv Appl Mech 7:55
22. Li XD, Nardi P, Baek CW, Kim JM, Kim YK (2005) J Micromech Microeng 15(3):551